Multirate Synchronous Sampling of Sparse Multiband Signals

Michael Fleyer, Alexander Linden, Moshe Horowitz, and Amir Rosenthal

***Abstract*—Recent advances in electro–optical systems make them ideal for undersampling multiband signals with very high carrier frequencies. In this paper, we propose a new scheme for sampling and reconstructing of a multiband sparse signals that occupy a small part of a given broad frequency range under the constraint of a small number of sampling channels. The locations of the signal bands are not known *a priori*. The scheme, which we call synchronous multirate sampling (SMRS), entails gathering samples synchronously at few different rates whose sum is significantly lower than the Nyquist sampling rate. The signals are reconstructed by finding a solution of an underdetermined system of linear equations by applying a pursuit algorithm and assuming that the solution is composed of a minimum number of bands. The empirical reconstruction success rate is higher than obtained using previously published multicoset scheme when the number of sampling channels is small and the conditions for a perfect reconstruction in the multicoset scheme are not fulfilled. The practical sampling system which is simulated in our work consists of three sampling channels. Our simulation results show that a very high empirical success rate is obtained when the total sampling rate is five times higher than the total signal support of a complex signal with four bands. By comparison, a multicoset sampling scheme obtains a very high empirical success rate with a total sampling rate which is three times higher than the total signal support. However, the multicoset scheme requires 14 channels.**

***Index Terms*—Analog–digital conversion, discrete Fourier transforms (DFTs), least squares methods, matrix inversion.**

I. Introduction

In many applications of radars and communications systems, it is desirable to reconstruct a multiband sparse signal from its samples. When the carrier frequencies of the signal bands are high compared to the overall signal width, it is not cost effective and often it is not feasible to sample at the Nyquist rate. It is therefore desirable to reconstruct the signal from samples taken at rates lower than the Nyquist rate. Recent advances in electro–optical systems enable undersampling of multiband sparse signals with carrier frequencies that can be located in a very broad frequency region (0–20 GHz) [1]. Such a broad bandwidth cannot be obtained in the current electronic technology. To exploit the advantages of optical sampling systems the undersampling should be performed using a small number of channels operating at high sampling rates. Moreover, there is an inherent advantage to sampling, in each channel, near the maximum sampling rate allowed by cost and technology. This is because sampling at higher rates increases the signal-to-noise ratio in the sampled signals [2].

There is a vast literature on reconstructing multiband signals from undersampled data [3]–[7]. Most of the methods are based on a multicoset sampling scheme. In a multicoset sampling scheme, m low-rate cosets are chosen out of L cosets of samples, obtained from time uniformly distributed samples taken at a rate F which is greater than or equal to the Nyquist rate F_{Nyq} [5]. In each channel, the sampling is offset by a different predetermined integer multiple of the reciprocal of the rate F. The data from the different sampling channels are then used to reconstruct a signal by solving a system of linear equations.

In [4], the problem of blind multiband signal reconstruction was first presented and solved by using a multicoset sampling scheme. In a blind signal reconstruction, the frequency support of the signal is not known *a priori*. Under certain conditions on the sampling rate and the number of channels, a proper choice of the time offsets between the sampling channels ensures a unique reconstruction in case that the signal bands locations are known *a priori* [5], or unknown *a priori* [4], [6], [7].

The main advantage of a multicoset sampling scheme is the ability to construct a universal sampling pattern [5], [7]. The algorithms for blind signal recovery of [7] and the sufficient conditions for their success rely on this property. However, in order to obtain a high success rate, the sampling should be performed using high number of sampling channels. Moreover, in order to obtain the theoretical minimum sampling rate, the bandwidth of the signal bands should be equal.

In this paper, we propose a different sampling and reconstruction strategy. The sampling is performed at P different rates each of which is an integer multiple of a basic sampling rate. The sampling of all channels starts simultaneously at a given time $t = 0$. We call this scheme a synchronous multirate sampling (SMRS) scheme. In a previous work [2], an algorithm for blind multiband signal reconstruction using asynchronous multirate sampling (MRS) scheme is described. That sampling scheme has been successfully implemented in experiments [10]. The main advantage of the asynchronous sampling scheme is that it does not require the knowledge of the time offset between the sampling channels. Hence, the hardware for the implementation becomes simple and the sampling is robust to errors in sampling times. This is because each sampling channel can be implemented separately without synchronization to other chan-

Manuscript received December 17, 2008; accepted September 12, 2009. First published October 20, 2009; current version published February 10, 2010. The associate editor coordinating the review of this manuscript and approving it for publication was Dr. Chong-Meng Samson See.

M. Fleyer, A. Linden, and M. Horowitz are with the Technion—Israel Institute of Technology, Haifa 32000, Israel (e-mail: mikef@tx.technion.ac.il; alinden@ee.technion.ac.il; horowitz@ee.technion.ac.il).

A. Rosenthal is with the Institute for Biological and Medical Imaging (IBMI), Technische Universitaet and Helmholtz Zentrum Muenchen, Neuherberg, Munich 85764, Germany (e-mail: eeamir@tx.technion.ac.il).

Color versions of one or more of the figures in this paper are available online at http://ieeexplore.ieee.org.

Digital Object Identifier 10.1109/TSP.2009.2034906

nels. An accurate reconstruction of the discretized signal spectrum by using this scheme requires that each frequency of the support of the signal be unaliased in at least one of the sampling channels. On the other hand, an SMRS scheme can reconstruct a signal in many cases. Included is the case that each part of the signal is unaliased in at least one channel; the condition of success in the unsychronized scheme [2]. In addition, an SMRS scheme can also reconstruct signals in other cases as well. This is because by using a system of linear equations aliased signals can often be reconstructed. However, synchronization requires that errors in the sampling time between the different channels as well as the differences between the transfer functions of the sampling channels be kept extremely small.

The Fourier transform of the undersampled signals is related to the original signal through an underdetermined system of linear equations that is described with a binary sampling matrix. With an asynchronous sampling scheme no such linear system exists.

We provide sufficient conditions for a unique recovery of the multiband signal locations and, consequently, the signal itself based on the assumption that the original signal is the sparsest solution among all signals that yield the same sampled data. However, these sufficient conditions require the use of many sampling channels. Therefore, such a scheme is impractical. In the scheme described in this paper, we use fewer channels thus sacrificing the sufficient conditions. Instead of assuming that the original signal is the sparsest we assume that the original signal is band sparse. This assumption is different from the one used to obtain sufficient conditions. However, it allows us to attain a high empirical reconstruction success rate using few sampling channels.

The sampling pattern of the SMRS scheme can also be obtained by using an equivalent multicoset sampling scheme. However, since the required time shifts between different sampling channels is very small, such a scheme cannot be practically implemented. Moreover, the number of channels in the equivalent multicoset sampling scheme is very high (on the order of 55 in one of our practical examples). The equivalent multicoset scheme enabled us to compare the empirical reconstruction success rate of SMRS to the reconstruction methods in [7] for the practical problem studied in this manuscript. In [7], two algorithms denoted by SBR4 and SBR2 are given for a blind reconstruction of sparse multiband signal. Since the sampling pattern in the equivalent multicoset scheme was not a universal pattern, we could not implement the algorithm described in SBR2 that enables a perfect reconstruction by using fewer sampling channels than required in SBR4 algorithm. We have implemented the SBR4 algorithm and compared its performance to our reconstruction method. The reconstruction method described in this manuscript gives a higher empirical reconstruction success rate than obtained by using SBR4 algorithm for four bands complex-valued signals and for real signals with a total bandwidth that is less than one fifth of the total sampling rate. The higher success rate is obtained since when the sampling rate in each channel is high, the probability that a sparse signal aliases simultaneously in all sampling channels becomes very low in the SMRS scheme. It is lower than in a multicoset sampling scheme in which, because all channels sample at the same frequency, an alias in one channel is equivalent to an alias in all channels. A universal sampling pattern that ensures a perfect reconstruction in a multicoset sampling scheme [5] can be obtained with a lower total sampling rate than required by the SMRS scheme. However, such a scheme requires a higher number of channels than is required in the SMRS scheme to achieve comparable empirical reconstruction success rate. This number can be prohibitively high, rendering such a sampling scheme impractical when implemented with electro–optical systems.

II. Synchronous Multirate Sampling

In this section, we describe a general synchronous multirate sampling. Let $F_{\max}$ be an assumed maximum carrier frequency and let $X(f) \in L^2([0, F_{\max}])$ be the Fourier transform of a complex-valued signal $x(t)$ that is to be reconstructed from its samples. Throughout the analysis, we calculate the Fourier transform by

$$X(f) = \int_{-\infty}^{\infty} x(t) e^{-j2\pi ft}\, dt.$$

The modifications required to reconstruct real-valued signals are described in Appendix I. We assume that the signal $x(t)$ to be sampled, in addition to being bandlimited in the frequency range $[0, F_{\max}]$, is multiband; i.e., the support of its Fourier transform is contained within a finite disjoint union of intervals $(a_n, b_n]$, each of which is contained in $[0, F_{\max}]$. By assumption, $\max b_n \leq F_{\max}$.

We also assume that the signal is sparse in a frequency domain; i.e., its spectral support is contained within N intervals $(a_i, b_i]$, where $\sum_{k=1}^{N} (b_k - a_k) \ll F_{\max}$.

In the SMRS scheme, the signal is sampled at P different sampling rates F_i $(i = 1 \ldots P)$. The signals, modulated by an optical pulses train at ith channel $x_i(t)$, are given by

$$x_i(t) = x(t) \sum_{n=-\infty}^{\infty} \delta\left(t - \frac{n}{F_i}\right) \tag{1}$$

where $\delta(t)$ is a Dirac delta "function." The Fourier transform $X_i(f)$ of the sampled signal in the ith channel satisfies

$$X_i(f) = F_i \sum_{n=-\infty}^{\infty} X(f + nF_i). \tag{2}$$

It follows from (2) that all the information about the sampled Fourier transform $X_i(f)$ is contained in the interval $[0, F_i]$. We refer to this interval as the ith baseband.

In our sampling scheme, each sampling rate is an integer multiple M_i of a basic frequency resolution Δf

$$F_i = M_i \Delta f. \tag{3}$$

For each $0 \leq f \leq F_{\max}$, we define an integer k and scalar $\beta, 0 \leq \beta < \Delta f$, such that $f = k\Delta f + \beta$. Equation (2) becomes

$$\begin{aligned} X_i(k\Delta f + \beta) &= F_i \sum_{n=-\infty}^{\infty} X(k\Delta f + \beta + nM_i\Delta f) \\ &= F_i \sum_{n=-\infty}^{\infty} X((k + nM_i)\Delta f + \beta). \end{aligned} \tag{4}$$

For each β and k, we define

$$X_i^k(\beta) = X_i(k\Delta f + \beta)$$
$$X_k(\beta) = X(k\Delta f + \beta). \quad (5)$$

Using these definitions, the Fourier transform of the sampled signal at the ith channel becomes

$$X_i^k(\beta) = F_i \sum_{n=-\infty}^{\infty} X_{k+nM_i}(\beta). \quad (6)$$

By using the same frequency resolution Δf for all the sampling channels we are able to construct a system of linear equations that allows reconstruction of the Fourier transform of the signal. By defining $M = \lceil F_{\max}/\Delta f \rceil$ to be the number of cells in the support of the original signal $X(f)$, (6) becomes

$$X_i^k(\beta)/F_i = \sum_{l=0}^{M-1} X_l(\beta) \sum_{n=-\infty}^{\infty} \delta[l - (k + nM_i)]. \quad (7)$$

Equation (7) can be written as a matrix equation. We define an $M_i \times M$ matrix $\mathbf{Q}_i$ whose elements are given by

$$(\mathbf{Q}_i)_{k+1,l+1} = \sum_{n=-\infty}^{\infty} \delta[l - (k + nM_i)],$$
$$0 \le k \le M_i - 1, \qquad 0 \le l \le M - 1. \quad (8)$$

Each element of $\mathbf{Q}_i$ is equal to either 1 or 0. This is because there is at most one contribution in the infinite sum of δ's which is made when $l \equiv k (\mathrm{mod}\ M_i)$. Moreover, $\mathbf{Q}_i$ is independent of β and the signal $\mathbf{x}(\beta)$. It depends only on the sampling rates and frequency resolution.

The vectors $\mathbf{x}_i(\beta)$ and $\mathbf{x}(\beta)$ are given by

$$(\mathbf{x}_i(\beta))_{k_i} = X_i^{k_i}(\beta)/F_i, \qquad 1 \le k_i \le M_i$$
$$(\mathbf{x}(\beta))_l = X_l(\beta), \qquad 1 \le l \le M. \quad (9)$$

By substituting (8) and (9) into (7) we obtain a system of linear equations for ith channel

$$\mathbf{x}_i(\beta) = \mathbf{Q}_i \mathbf{x}(\beta). \quad (10)$$

For each value of i ($i = 1 \ldots P$), (10) defines a set of linear equations that relate the Fourier transform of the signal to the Fourier transform of its samples. The vector $\mathbf{x}(\beta)$ in (10) is the same for all the P equations because it does not depend on the sampling. Therefore, we can construct a single system of linear equations

$$\hat{\mathbf{x}}(\beta) = \hat{\mathbf{Q}} \mathbf{x}(\beta) \quad (11)$$

where the vector $\hat{\mathbf{x}}(\beta)$ and the matrix $\hat{\mathbf{Q}}$ are obtained by concatenating the vectors $\mathbf{x}_i(\beta)$ and matrices $\mathbf{Q}_i$ as follows:

$$\hat{\mathbf{x}}(\beta) = \begin{pmatrix} \mathbf{x}_1(\beta) \\ \mathbf{x}_2(\beta) \\ \vdots \\ \mathbf{x}_P(\beta) \end{pmatrix} \quad \hat{\mathbf{Q}} = \begin{pmatrix} \mathbf{Q}_1 \\ \mathbf{Q}_2 \\ \vdots \\ \mathbf{Q}_P \end{pmatrix}.$$

The matrix $\hat{\mathbf{Q}}$ has exactly P nonvanishing elements in each column. These correspond to the locations of the spectral replica in each channel baseband. We note that the matrix $\hat{\mathbf{Q}}$ is different from that used in the multicoset sampling scheme [5]. In the SMRS scheme, the sampling matrix is binary, whereas in the multicoset sampling scheme, the sampling matrix is a submatrix of some discrete Fourier transform (DFT) matrix and thus contains complex exponentials.

To invert (11) and calculate the signal Fourier transform $\mathbf{x}(\beta)$, it is necessary that the number of rows $\sum_{i=1}^{P} M_i$ in $\hat{\mathbf{Q}}$ be equal to or larger than the number of columns M. Defining $F_{\text{total}} = \sum_{i=1}^{P} F_i$ makes this condition equivalent to the condition

$$F_{\text{total}} > F_{\max}. \quad (12)$$

The condition on the sampling rates given in (12) is consistent with the requirement that the sampling rate be greater than the Nyquist rate of a general signal whose spectral support is $[0, F_{\max}]$. However, when sampling sparse signals, an inversion of the matrix may be possible even if the condition (12) is not fulfilled. Our objective is to invert (11) in the case of sparse signals with sampling rates $F_{\text{total}} < F_{\max}$.

III. Inversion Algorithm

In this section, we describe the inversion algorithm for the SMRS scheme assuming a sparse signal with unknown signal bands locations. The purpose of the algorithm is to invert (11); i.e., to calculate the vector $\mathbf{x}(\beta)$ from the vector $\hat{\mathbf{x}}(\beta)$.

We denote by $\mathbf{S}$ the set of matrix columns that correspond to the possible support of a signal, and by $\hat{\mathbf{Q}}_{\mathbf{S}}$ the matrix with the corresponding columns. The resulting system of equations that relate the original signal to the sampled signal is

$$\hat{\mathbf{x}}(\beta) = \hat{\mathbf{Q}}_{\mathbf{S}} \mathbf{x}_{\mathbf{S}}(\beta) \quad (13)$$

where $\mathbf{x}_{\mathbf{S}}(\beta)$ contains only elements defined by $\mathbf{S}$. By inverting (13), it is possible to reconstruct the original signal cells vector $\mathbf{x}_{\mathbf{S}}(\beta)$ for any frequency β. The reconstruction is unique when the matrix $\hat{\mathbf{Q}}_{\mathbf{S}}$ has a full column rank.

Without the knowledge of the signal support $\mathbf{S}$, a unique inversion of (11) is not possible in the general case, since the original matrix $\hat{\mathbf{Q}}$ is not full column rank. However, if the desired signal vector $\mathbf{x}(\beta)$ is assumed to be sparse for each β, then we obtain the optimization problem

$$\mathbf{x}^*(\beta) = \arg \min_{\mathbf{x}(\beta)_{\text{s.t. }} \hat{\mathbf{x}}(\beta) = \hat{\mathbf{Q}}\mathbf{x}(\beta)} ||\mathbf{x}(\beta)||_0. \quad (14)$$

This is a standard problem of compressed sensing and the sufficient conditions for obtaining a unique solution of (14) were studied in several works (see [9], for example). In Section III-A, we provide sufficient conditions for the SMRS scheme to recover a unique solution using the sparsity assumption on the original signal.

A. Sufficient Perfect Reconstruction Conditions for Sparsest Signal Recovery

The conditions on the existence of the sparsest solution of the underdetermined system of linear equations such as (14) can be found by using the *spark* [9] of the sampling matrix.

The *spark* of a given matrix $\mathbf{Q}$ is the smallest number of columns of $\mathbf{Q}$ that are linearly dependent. For a universal sampling pattern, the spark of a sampling matrix is equal to the

number of the sampling channels P plus one [5]; i.e., any submatrix created by selecting any set of P columns of the sampling matrix has full column rank.

The unique solution of (14) is guaranteed if the spark of the matrix $\hat{\mathbf{Q}}$ is at least twice the sparsity of the solution vector $\mathbf{x}(\beta)$ [9]. Calculating the exact value of the spark of $\hat{\mathbf{Q}}$ may be practically impossible, but a lower bound can be obtained by calculating the mutual coherence—μ (see [9, Lemma 1]). The mutual coherence of a given matrix $\mathbf{A}$ is the largest absolute normalized inner product between different columns from $\mathbf{A}$. According to [9, Th. 2], a unique sparsest solution of (11) exists if $\|\mathbf{x}\|_0 < (1/2)(1+1/\mu)$. This gives us a lower bound theoretical condition for perfect reconstruction of the SMRS scheme. By choosing P channels whose frequencies satisfy $F_{\max} < \mathrm{lcm}(M_i, M_j)\Delta f$, we obtain $\mu = 1/P$ (lcm stands for the least common multiple).

We choose $P \geq 2N$ where N is the maximum number of bands with maximum width Δf. Set the sampling rates of the channels be equal to $F_i = M_i \Delta f$, where the integers M_i are chosen to satisfy $F_{\max} < \mathrm{lcm}(M_i, M_j)\Delta f$ for each pair of channels $1 \leq i, j \leq P$. Therefore, by [9, Th. 2], the unique solution of (14) is guaranteed for $\|\mathbf{x}(\beta)\|_0 \leq P$.

Notice that the multiple measurements vector (MMV) system of linear equations (15) can be solved separately for each β_n. Then, a unique sparsest solution $\mathbf{x}(\beta_n)$ exists for each one of the equations. There are several known methods such as *orthogonal matching pursuit* or *basis pursuit* [9] for obtaining a sparsest solution to an underdetermined system of equations. For both methods, the sufficient condition for obtaining a unique sparsest solution to (14) is that $\|\mathbf{x}\|_0 < (1/2)(1+1/\mu)$ [9, Th. 3 and 4]. Therefore, the theoretical sufficient condition also guarantees that practical algorithms converge to the right solution under the requirements we impose on the original signal and on the sampling scheme.

Our sufficient conditions do not take into account the reduction procedure and the assumption that the signal is composed of the minimum number of bands. These assumptions will be introduced in the sequel. Our simulations results show that empirical reconstruction success rate that is close to unity is obtained even when our sufficient conditions on the number of the samplers and their sampling rates are not satisfied.

B. SMRS Scheme Implemented With a Small Number of Sampling Channels

In this work, we assume that the signal or the sampling time window are finite as occurs in practical applications. The resulting finite-time signal can no longer be considered as a multiband signal in a strict sense since its spectrum does not equal to zero over closed intervals. Since time-limited signals are sampled within a finite time window they are completely characterized by their DFT sequence. We assume that the signal can be accurately reconstructed by using only few significant spectrum components and by discarding small ones. Similar assumption is commonly used in the field of compressed sensing for representing signals in a general orthogonal basis [8]. In practice, the small spectrum coefficients that are below some threshold can be discarded without significantly effecting the original signal. Moreover, in practical systems, the dynamic range is limited due to noise and distortions, and therefore, a threshold is used to eliminate small frequency components that are below the sensitivity of the system.

In multirate sampling scheme, the sampling frequencies are multiple of a basic frequency resolution Δf (3). The basic frequency resolution Δf defines the width of each frequency cell of the original and the sampled signal vectors $\mathbf{x}(\beta)$ and $\mathbf{x}_i(\beta)$, respectively. Since we restrict ourself to a discrete signal problem, we discretize the continuous variable β of the system of (11). There is no unique way for choosing the discrete value of β. However, by selecting a time window with a duration $1/\Delta f$ and calculating the DFT of the sampled sequences, we obtain a discrete spectrum at frequencies that correspond to a single sample that is taken in each frequency cell. Therefore, the discretized β equals 0. When the duration of the time window is longer than $1/\Delta f$, it is also possible to calculate the spectrum with the required resolution $1/\Delta f$. One could increase the frequency resolution by choosing a window duration of $N/\Delta f$, where N is an integer number. This would result in a system of equations known as an MMV

$$[\hat{\mathbf{x}}(\beta_1) \ldots \hat{x}(\beta_N)] = \hat{\mathbf{Q}}[\mathbf{x}(\beta_1) \ldots \mathbf{x}(\beta_N)] \tag{15}$$

where $\beta_n = (n-1)\Delta f/N$, $1 \leq n \leq N$. The solution of such system of equations can be obtained by extending the algorithm described in this manuscript. In the rest of this paper, we assume that the frequency resolution of the discrete spectrum equals Δf and the discretized value of β equals zero.

Because we are using fewer channels than are required to guarantee a solution, we require that the signal $\mathbf{x}$ possesses some mathematical properties. These properties are necessary for successful blind signal reconstruction using the SMRS scheme with small number of the sampling channels.

Property 1—Multiband: The DFT of the signal consists of a number of bands $(a_n, b_n]$ that lie inside a region $[0, F_{\max}]$, where $F_{\max}$ is known *a priori*. A band is defined as a sequence of nonzero amplitude values in the discrete Fourier domain.

The maximum frequency $F_{\max}$ fulfills the requirement $F_{\max} < \mathrm{lcm}(M_1, \ldots, M_P)\Delta f$. This requirement is explained in Section III-C that describes the reduction procedure.

Property 2—Sparse: The signal is sparse; i.e., $\sum_{n=1}^{N}(b_n - a_n) \ll F_{\max}$. In the discrete problem, the number of nonzero values in the signal DFT vector $\mathbf{x}$ must be small compared to the maximum vector length ($\|x\|_0 \ll M$). This property is essential since we are looking for a sparse solution of the underdetermined system of linear equations (11).

Property 3—Minimal Bands: We require that the original signal contains the minimum number of bands among all the signals that result in the same sampled data $\hat{\mathbf{x}}(\beta)$. Therefore, we assume that the signal has a band-sparse structure that is different from a regular sparsity assumption used in our sufficient reconstruction conditions. In Section III-C, we propose a reduction scheme that provides a band-structure model for each sampled signal.

Property 4—Uniqueness: There are cases in which the knowledge of the signal support is not sufficient for signal reconstruction. This occurs when the sampling matrix $\hat{\mathbf{Q}}_{\mathrm{org}}$

corresponding to the original signal $\mathbf{x}_{\text{org}}$ is not full column rank. A unique solution to

$$\hat{\mathbf{x}}_{\text{org}} = \hat{\mathbf{Q}}_{\text{org}}\mathbf{x}_{\text{org}} \tag{16}$$

exists only if $\hat{\mathbf{Q}}_{\text{org}}$ has full column rank [11].

Therefore, we assume that the original sampled signal corresponds to a full column rank matrix and the solution exists provided the signal support.

Property 5—Aliasing: We assume that in the absence of noise a zero value in a baseband signal frequency corresponds to a zero value in all the frequencies in the original signal that are downconverted to that frequency; i.e., $X_i^k = 0$ if and only if $\mathbf{x}_{k+nM_i} = 0$ for all $0 \le n < M/M_i$. This assumption does not hold for specific signals in which two (or more) different frequency components completely cancel each other due to aliasing. Clearly, in the noiseless environment, the probability of this happening is zero. However, in a noisy environment, this assumption is not always fulfilled since a threshold on the sampled signals has to be defined. We analyze this case in Appendix III.

C. Reduction Procedure

By observing the sampled signals, one can detect baseband frequencies in which there is no signal. These baseband frequencies can be used together with Property 5 to eliminate originating frequencies and thus to reduce the matrix in (11). The elimination is similar to one described in asynchronous MRS [2]. In Appendix II, we rigorously describe the mathematical mechanism behind the reduction procedure.

We define the indicator function $\chi_i[l]$ as follows:

$$\chi_i[l] = \begin{cases} 1, & \text{for all } l \in [0, M-1] \text{ such that } X_i(l\Delta f) \neq 0 \\ 0, & \text{otherwise.} \end{cases} \tag{17}$$

The function $X_i(f)$ is periodic with period F_i. Therefore, $\chi_i[l]$ is a periodic extension of an indicator function over the baseband $f \in [0, F_i)$.

We define the $\chi[l]$ as follows:

$$\chi[l] = \prod_{i=1}^{P} \chi_i[l], \qquad l \in [0, M-1]. \tag{18}$$

The function $\chi[l]$ equals 1 over the intersection of all the upconverted bands of the P sampled signals and it defines the columns of the matrix $\hat{\mathbf{Q}}$ that are retained in forming the reduced matrix $\hat{\mathbf{Q}}_{\mathbf{S}}$. All other columns are eliminated and their corresponding elements in the vectors $\mathbf{x}$ are also eliminated. After the elimination of the columns from the matrix $\hat{\mathbf{Q}}$, the matrix rows that correspond to zero elements in $\hat{\mathbf{x}}$ and their corresponding elements in the vectors $\hat{\mathbf{x}}$ are also eliminated.

The reduction process is demonstrated in Fig. 1 for a two-band complex signal and two sampling channels. The upconverted supports of the sampled signals at sampling frequencies F_1 and F_2 are denotes by χ_1 and χ_2, respectively. Two signal bands overlap in the first sampling channel. The possible signals

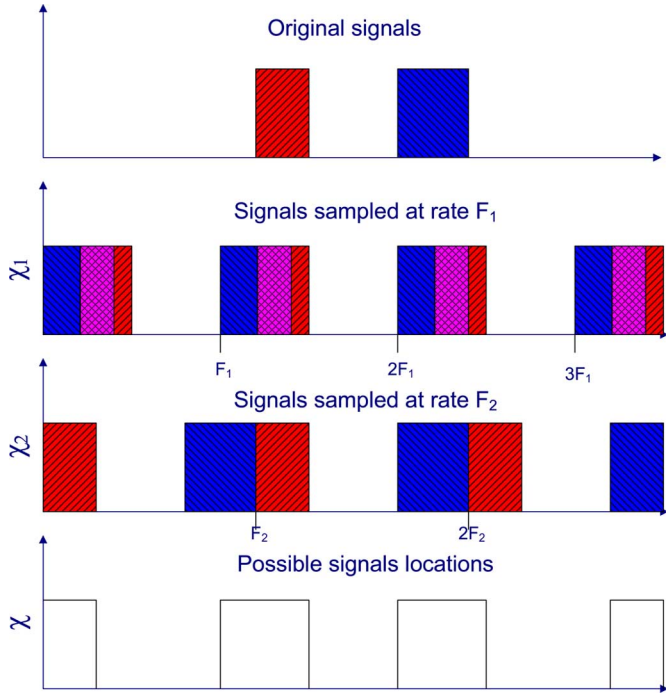

Fig. 1. Demonstration of the reduction procedure. Signals sampled at rate F_i contain all possible replicas of the original signal. Possible signals locations are the intersection between the supports of the possible signals sampled at rates F_1 and F_2. In channel 1, the pink color denotes overlapping of signal supports.

locations are described by the function χ which is the intersection of χ_1 and χ_2. The idea behind the reduction procedure is also explained in Appendix II.

In some cases, the function $\chi[l]$ equals 1 only for frequencies within the spectral support of the signal. In such cases, the resulting equations are identical to those found in Section III-B [see (16)]. However, in other cases, as shown in Fig. 1, $\chi[l]$ may also equal 1 for frequencies outside the true signal spectral support. In such cases, the reduced matrix will have more columns than the matrix obtained in the case in which the spectral support of the signal is known ($\hat{\mathbf{Q}}_{\text{org}}$). As a result, the inversion requires finding the values of more variables.

Each eliminated zero energy baseband component causes elimination of respective rows and columns. The elimination of one baseband entry means that all the frequencies that are downconverted to that baseband entry (the aliasing frequencies) are also eliminated. This is because of our Property 5: zero entry in the baseband corresponds to zero entries in all of the frequency components of the original signal that are downconverted to frequency of the baseband entry. Therefore, elimination of one baseband entry results in elimination of $\lfloor F_{\max}/\min\{F_i\} \rfloor$ to $\lceil F_{\max}/\max\{F_i\} \rceil$ corresponding columns. Thus, if the number of the zero elements in $\hat{\mathbf{x}}$ is sufficiently large, the number of rows in the matrix $\hat{\mathbf{Q}}_{\mathbf{S}}$ may be larger than the number of columns.

If in addition, matrix $\hat{\mathbf{Q}}_{\mathbf{S}}$ has a full column rank, the problem is either consistent or overdetermined. In such cases, there is a unique inversion to the reduced system of linear equations which can be found using the Moore–Penrose pseudoinverse. If the matrix is not full column rank, the problem is underdetermined and the inversion is not unique. A unique solution in

such cases can be obtained either by increasing the total sampling rate or by adding additional assumptions on the signal.

The choice of sampling rates imposes restrictions on the possible values of $F_{\max}$ for which an inversion of the reduced system of linear equations is possible. For the matrix $\hat{\mathbf{Q}}_{\mathbf{S}}$ to have full column rank, it must not have any identical columns. Since we do not restrict the possible locations of the known signal bands, any combination of columns of the matrix $\hat{\mathbf{Q}}$ may appear in the matrix $\hat{\mathbf{Q}}_{\mathbf{S}}$. Therefore, we require that $\hat{\mathbf{Q}}$ not have any identical columns. The matrix $\hat{\mathbf{Q}}$ is composed of P submatrices $\mathbf{Q}_i$ whose columns are periodic

$$(\mathbf{Q}_i)_{k,l+M_i} = (\mathbf{Q}_i)_{k,l}.$$

For the matrix $\hat{\mathbf{Q}}$ not to be periodic, it is required that any common period of the P submatrices be larger than M. This condition is met if the least common multiple of the $\{M_i\}_i$ is larger than M. As a result, $F_{\max}$ should fulfill $F_{\max} < \operatorname{lcm}(M_1, \ldots, M_P)\Delta f$.

D. Ill-Posed Cases

In many cases, the matrix $\hat{\mathbf{Q}}_{\mathbf{S}}$ for unknown band locations is not full column rank. In these cases, there are subsets of matrix columns that are linearly dependent. Using this linear dependence, a solution to the reduced system of linear equations can be found. However, any solution found can be used to construct an infinite number of solutions to the equation. Thus, there is no unique solution and the inversion problem is ill-posed.

We attempt to reconstruct a signal in the case in which the inversion problem is ill-posed by applying Property 3. Since the original signal is multiband, possible signal locations have a band structure as explained in Appendix II. Under the assumptions stated earlier (the assumption that leads to matrix reduction, the existence of the unique solution to (16) when the signal bands are known, and band sparsity) the inversion problem is reduced to finding the solution of the reduced system of linear equations that is composed of the minimum number of bands. The problem is NP-hard since we need to test every possible combination of bands.

The algorithm described here is of lower complexity and its purpose is to find a solution that is composed of the minimum number of bands without testing all the combinations. The resulting algorithm attains a lower success rate but decreases the runtime significantly as compared to an NP-complex algorithm. We do not provide the conditions under which the correct solution is obtained.

Our algorithm is based on the orthogonal matching pursuit (OMP) [9]. This algorithm belongs to the category of the "greedy search" algorithms. The original OMP algorithm is used to find the sparsest solution $\mathbf{x}$ of underdetermined equations $\tilde{\mathbf{Q}}\mathbf{x} = \mathbf{b}$ [9] where $\tilde{\mathbf{Q}}$ is an underdetermined matrix. The sparsest solution is the solution having the smallest norm $||\mathbf{x}||_0$ where $||\mathbf{x}||_0$ is the number of nonzero elements in the vector $\mathbf{x}$. The original OMP algorithm collects columns of the matrix $\tilde{\mathbf{Q}}$ iteratively to construct a reduced matrix $\tilde{\mathbf{Q}}_{\mathrm{r}}$. At each iteration n, the column of $\tilde{\mathbf{Q}}$ which is added to $\tilde{\mathbf{Q}}_{\mathrm{r}}^{n-1}$ to produce a matrix $\tilde{\mathbf{Q}}_{\mathrm{r}}^{n}$ is the column which results in the smallest residual error $\min_{\mathbf{x}} ||\mathbf{b} - \tilde{\mathbf{Q}}_{\mathrm{r}}^{n}\mathbf{x}||_2^2$ where for every vector $\mathbf{y}$, $||\mathbf{y}||_2^2 = \sum_i y_i^2$. The iterations are stopped when some threshold ϵ is achieved. Sufficient conditions are given for the algorithm to obtain the correct solution [9].

We denote $\tilde{\mathbf{Q}} = \hat{\mathbf{Q}}_{\mathbf{S}}$, $\mathbf{b} = \hat{\mathbf{x}}_{\mathbf{S}}$, and $\mathbf{x} = \mathbf{x}_{\mathbf{S}}$. Since we are seeking the solution of $\tilde{\mathbf{Q}}\mathbf{x} = \mathbf{b}$ with the smallest number of bands and not the smallest norm $||\mathbf{x}||_0$, we modify the OMP algorithm. Instead of choosing a single column as in [9], we select iteratively blocks of columns. Each band that corresponds to sequence of ones of the function $\chi[l]$ identifies a possible band of the spectral support of the reconstructed signal. The columns of the matrix $\tilde{\mathbf{Q}}$ can be divided into J blocks. The jth band contains the index of columns B_j of the matrix $\tilde{\mathbf{Q}}$.

We start the iteration with the empty set $S^0 = \emptyset$ of column indexes, the empty matrix $\tilde{\mathbf{Q}}_{\mathrm{r}}^0$, and the set $B^0 = \bigcup_{j=1}^{J} B_j$, so that at nth iteration the following holds: $S^n \bigcup B^n = B^0$. At the nth iteration $(n > 1)$ the algorithm must decide which band to add to $\tilde{\mathbf{Q}}_{\mathrm{r}}^{n-1}$. If the index set B_j is chosen, then $S^n = S^{n-1} \cup B_j$ and $B^n = B^{n-1} \setminus B_j$. The matrix $\tilde{\mathbf{Q}}_{\mathrm{r}}^{n}$ is the matrix whose columns are selected from $\tilde{\mathbf{Q}}$ according to the indexing set S^n.

The band added is the one that produces the smallest residual error $\epsilon^n = \min_{B_j \in B^{n-1}} \min_{\mathbf{x}} ||\mathbf{b} - \tilde{\mathbf{Q}}_{\mathrm{r,j}}^{n}\mathbf{x}||_2^2$ where $\tilde{\mathbf{Q}}_{\mathrm{r,j}}^{n}$ is the matrix obtained by adding the band indexed by B_j to $\tilde{\mathbf{Q}}_{\mathrm{r}}^{n-1}$. The algorithm stops when the threshold ϵ is reached. The threshold ϵ is a very small number and reflects upon the finite numerical precision of the calculations.

The algorithm performed well in our simulations. However, there were rare cases in which the support of the reconstructed solution did not contain all the originating bands and rare cases in which the reconstructed signal was incorrect even though all the assumptions on a signals given in Section III-B were fulfilled. The algorithm failed primarily for one of two reasons. One of them was due to the inclusion of a band that reduced the residual error on the one hand, but on the other hand, caused a resulting matrix $\tilde{\mathbf{Q}}_{\mathrm{r}}^{n}$ to be not full column rank as hypothesized in our problem (in Section III-B). This can happen, for example, when a band consists of a correct subband and erroneous subblocks. Including any erroneous subblocks may result in an ill-posed problem. Another reason for failure was a large dynamic range of the signals. When reconstructing such signals, correct bands may be ignored by the algorithm in cases that the energy within the bands is significantly lower than the energy in other bands.

It is difficult to find adequate sufficient conditions for the modified OMP to succeed. There are two main reasons for this. First, in the previously described reduction procedure, different signals result in different reduced matrices and different band partitions. Second, because of aliasing or adjacency, the size of each band may be different. These situations occur even if the signal bands are of the equal size and the number of bands is constant, but their locations are varying. In our algorithm, we do not make any assumption on the signal band widths or their number.

IV. Simulations Results

The ability of the signal reconstruction algorithm to recover different types of signals was tested. In all of our simulations, it was assumed that there are only three sampling channels as used in our electro–optical system [10]. In the first set of simulations,

TABLE I
SIMULATION PARAMETERS

Signals	Complex	Real
Freq. range	[0,20] GHz	[-20,20] GHz
Sampling rates	0.95, 1.0, 1.05 GHz	3.8, 4.0, 4.2 GHz
Number of bands	4	8
Freq. range/F_{total}	$6\frac{2}{3}$	$3\frac{1}{3}$

TABLE II
EMPIRICAL SUCCESS RATES OBTAINED BY USING SMRS RECONSTRUCTION SCHEME AND BY USING SBR4 CALCULATED FOR FOUR-BAND COMPLEX SIGNALS AND FOR FOUR-BAND REAL SIGNALS

$\frac{F_{\text{total}}}{F_{\text{BW}}}$	Complex, SBR4	Complex, MRS	Real, SBR4	Real, MRS
3.5	96.66	99.48	90.31	81.41
4.0	97.70	99.39	93.64	92.34
4.5	98.59	99.77	95.30	95.15
4.8	98.93	99.91	96.30	96.66
5.0	99.10	99.88	96.51	96.92
5.8	99.40	99.97	97.94	98.64
6.0	99.69	99.95	98.01	98.81
6.5	99.53	99.99	98.67	99.19
7.5	99.76	100.00	99.19	99.54
10.0	99.91	99.99	99.50	99.95

the ability of the algorithm to reconstruct multiband complex and real-valued signals with different spectral supports, shapes, and bandwidths that were not known *a priori* was tested. Additional simulations were performed in which real-valued multiband signals were contaminated by additive white noise. Simulation parameters (frequency range, sampling rates, and number of signal bands) are shown in Table I. Band carrier frequencies were chosen from a uniform distribution over the maximum support. In different simulations, the width of each band (hence the total bandwidth of the signal) was varied. The reconstruction algorithm was unaware of the number of signal bands. In all the simulations, the frequency resolution was set to 5 MHz. For each set of simulations, we counted the mean rate of ill-posed cases in which the modified OMP algorithm had to be used to recover the signal. Mean times for accurate signal reconstruction were also recorded. Failures of the reconstruction were either because one of the initial assumptions given in the previous section was not fulfilled or because of the failure of the modified OMP algorithm.

Since the data obtained by the SMRS scheme can be also obtained by a multicoset sampling scheme, we compared the empirical success rate of our reconstruction algorithm to the success rate obtained using SBR4 scheme of [7]. We could not implement the algorithm described in SBR2 that enables a perfect reconstruction by using less sampling channels than required in SBR4 scheme since our sampling pattern is not universal. In order to obtain a universal sampling pattern as used in SBR2, the number of sampling channels should be significantly higher than 3.

The sampling rates F_i in our simulations were selected based on the constraints on the maximum sampling rate of the optical system [10]. In general, the sampling rates should be chosen to be as close as possible to the maximum sampling rate to achieve highest SNR as well as maximum total sampling rate. In addition, the necessary condition on the lcm of the sampling rates (see Property 1) must be applied. It can be easily shown that the effective sampling rate (number of samples per unit time) is bounded by

$$F_{\text{eff}} \leq \sum_{i=1}^{P} M_i \Delta f - (P-1)\mathrm{gcd}(M_1, \ldots, M_P)\Delta f \qquad (19)$$

where gcd is the greatest common divisor. To maximize the effective sampling rate rates should be chosen in a way that minimizes the number of sampling times common to more than one channel. This is achieved when the gcd is minimal. In addition, we require each F_i to be greater than the maximum possible signal support ($F_i > \sum_{k=1}^{N}(b_k - a_k)$). This is to increase the number of gaps in the baseband and thus to improve the reduction procedure.

In some choices of frequency rates, there are several values of the basic frequency resolution Δf that satisfy (3). If the maximum signal widths are known beforehand, this information can be used to choose Δf. Whereas a smaller Δf gives a higher success rate, too small value results in too large sampling matrix.

The simulations were performed on a 2-GHz Core2Duo central processing unit (CPU) with 2-GB RAM storage in the Matlab 7.0 environment (no special programming was performed to use both cores).

A. Ideal Multiband Signals

Since we assume sampling in a finite length time window we represent the signals in our simulations by their DFT. Therefore, the signals we use in our simulations are sparse in a discrete sense; i.e., most of the elements of the DFT of the signal sampled at the Nyquist rate are equal to zero. On the other hand, the continuous-valued Fourier transform of the same signal does not have zero energy in any band with a finite support due to the finite time window of the signal.

For ideal signals, the algorithm was evaluated by a perfect reconstruction criterion for the DFT sequence; i.e., a mean difference between the DFT of the original and the reconstructed signal is less than 10^{-10}. Whenever this error was attained, the reconstruction was deemed to have been successful. Otherwise, it was deemed to have failed. The threshold for the modified OMP was chosen accordingly: $\epsilon = 10^{-20}$.

The same data that are obtained using the SMRS scheme can always be obtained by a multicoset sampling scheme since the ratio between each pair of sampling rates is rational. However, in our examples, the number of the sampling channels in the equivalent multicoset scheme is significantly higher than in SMRS where only three sampling channels were used. The sampling rate of each coset is equal to $1/LT = 50$ MHz and the number of multicoset sampling channels (p) is equal to 58. The time offset between the cosets is a multiple of $T = 1/399$ GHz. The downsampling factor L is 399 GHz/50 MHz $= 7980$.

In the first set of simulations, we assumed complex signals to compare the results to those published using the multicoset sampling recovery scheme of [7]. Both the real and imaginary spectra of the signal within each band were chosen to be normally distributed. Specifically, for each frequency $f = k\Delta f$ in a chosen band, the real and imaginary components of $X(f)$ were chosen randomly and independently from a standard normal distribution. The amplitude of each bands' spectra was scaled by

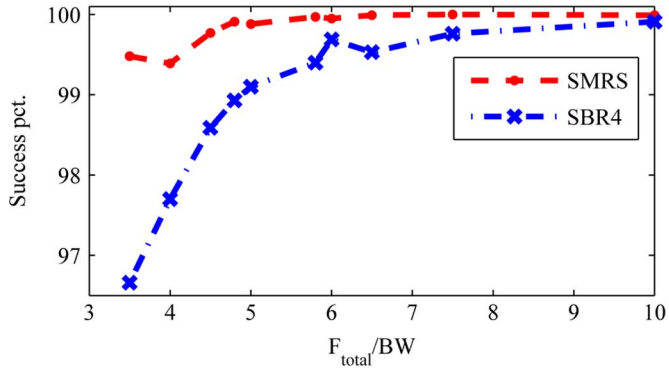

Fig. 2. Empirical success percentages for four-band complex signals calculated by using the SMRS reconstruction scheme (circles) and by using SBR4 in [7] (crosses) as a function of the spectral support (BW) for $F_{\text{Nyquist}} = 20$ GHz and a total sampling rate $F_{\text{total}} = 3$ GHz. The number of sampling channels is equal to 3 in the SMRS scheme and is equal to $p = 58$ in the equivalent multicoset sampling scheme.

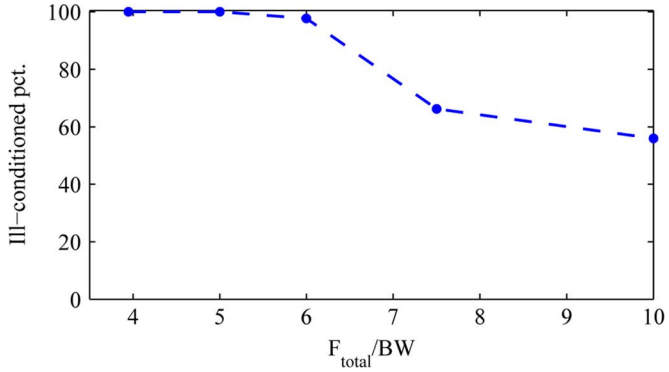

Fig. 3. Ill-posed cases mean percentage for four-band complex signals for different spectral supports (BW) with $F_{\text{Nyquist}} = 20$ GHz and a total sampling rate $F_{\text{total}} = 3$ GHz.

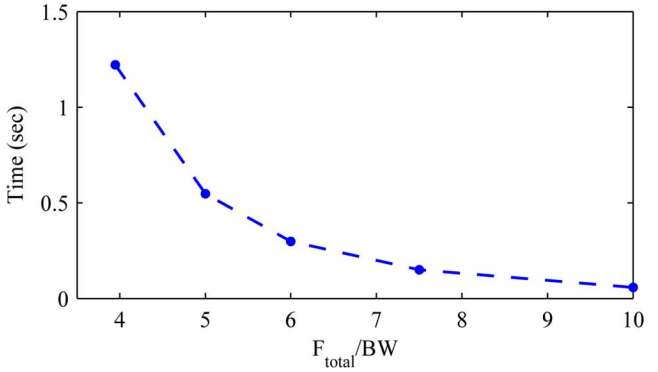

Fig. 4. Mean runtimes for four-band complex signals for different spectral supports (BW) with $F_{\text{Nyquist}} = 20$ GHz and a total sampling rate $F_{\text{total}} = 3$ GHz.

a constant α such that each band's energy was equal to a uniformly generated value E on the interval $[1, 5]$; i.e., for specific band

$$X(f) = \alpha[X_r(f) + jX_{im}(f)] \quad ||X(f)||_2 = E.$$

Identical DFTs of the signals were used to test the multicoset sampling reconstruction scheme of [7]. The empirical success rates were obtained for each bandwidth (BW) of the original signal DFT by using 10 000 runs. The success rates for the two reconstruction methods is shown in Fig. 2.

As is evident from Fig. 2, the empirical success percentage of an ideal reconstruction is high using the reconstruction method described in this manuscript when $F_{\text{total}}/\text{BW} \geq 5$. The empirical success rate is significantly higher than obtained by using SBR4 scheme of [7]. The results given in [7] shows that for $L = 23$ the empirical perfect reconstruction is achieved with at least six channels and with $F_{\text{total}}/\text{BW} > 13$. In the SMRS scheme, a very high empirical success rate was obtained using only three channels with a total sampling rate that obeys $F_{\text{total}}/\text{BW} \geq 5$. The total sampling rate in a multicoset scheme can be significantly lower than required in SMRS scheme. However, the number of channels that are used in that scheme is significantly higher compared to that used in SMRS where only three sampling channels are used. For example, in SBR2 scheme (downsampling factor $L = 199$) the empirical success rate was calculated for complex signals with four bands, each having a 100-MHz bandwidth. A very high reconstruction success rate was obtained for $F_{\text{total}}/\text{BW}$ greater than about 3. However, the number of sampling channels was $p = 14$ compared to only three channels in SMRS.

The mean percentage of ill-posed cases is shown in Fig. 3. The figure shows that for $4 \leq F_{\text{total}}/\text{BW} \leq 10$, in most of the tested cases, the matrix inversion was ill posed. Nonetheless, a very high success percentage was obtained for these cases. This indicates that our modified OMP algorithm was very successful in resolving these cases.

Fig. 4 shows the mean runtime as a function of $F_{\text{total}}/\text{BW}$ (constant total sampling rate and varying signal support). Because matrix inversion is the most computationally intensive operation in the algorithm, the mean runtime decreases as the signal bandwidth decreases. This is because, strictly speaking, with a fixed resolution, the matrix size monotonically depends on total signal bandwidth. Moreover, as the ratio $F_{\text{total}}/\text{BW}$ increases, the possible spectral support obtained at the first step of the reconstruction increases beyond the increase of the signal bandwidth.

The algorithm, modified as explained in Appendix I, was also tested against real-valued signals. The sampling frequencies are the same as are used in our optical experimental setup based on asynchronous MRS [2]. Each band was chosen to be of equal width BW/8. Once a band $(a, b]$ was chosen, the Fourier transform of $X(f)$ for $f \in (a, b]$ was determined by the following formula:

$$X(f) = A \sin\left[\frac{\pi(f-a)}{b-a}\right] e^{j2\pi \sin\left[\frac{\pi(f-a)}{b-a}\right] + j\theta}$$
$$X(-f) = X^*(f). \tag{20}$$

The phase θ was chosen randomly from a uniform distribution on $[0, 2\pi]$ and the amplitude A was chosen randomly from a uniform distribution on $[1, 1.2]$.

Fig. 5 shows the empirical success rate of the algorithm tested against real-valued signals. As is evident from the figure, the empirical success rate is high when $F_{\text{total}}/\text{BW} \geq 8$. We note that the required sampling rate is significantly higher in this example than in the complex signals simulation. The reason is that in the real case example there are twice as many bands as in the complex case simulations. Hence, after the sampling, an overlap may also occur between the negative and positive bands of the real signal. We note that when sampling a real signal at a sampling rate F_i, it is sufficient to know the Fourier transform in

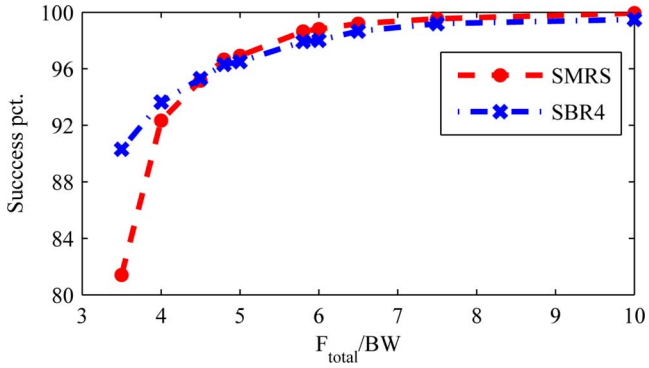

Fig. 5. Empirical success percentages for equal four-band real signals calculated by using the SMRS reconstruction scheme (circles) and by using SBR4 in [7] (crosses) as a function of the spectral support (BW) for $F_{\text{Nyquist}} = 40$ GHz and a total sampling rate $F_{\text{total}} = 12$ GHz. The number of sampling channels is equal to 3 in the SMRS scheme and is equal to $p = 58$ in the equivalent multicoset sampling scheme.

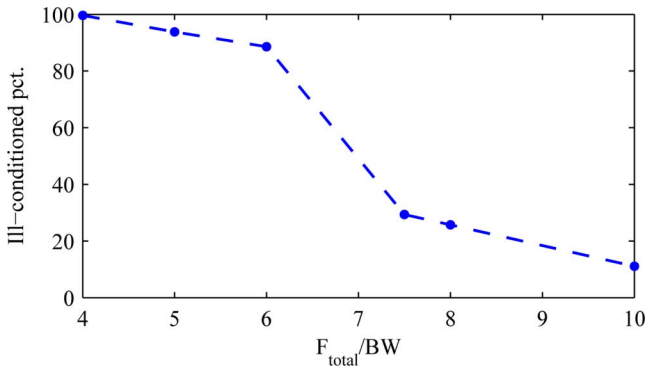

Fig. 6. Ill-posed cases mean rate for four-band real signals for different spectral supports (BW) with $F_{\text{Nyquist}} = 40$ GHz and a total sampling rate $F_{\text{total}} = 12$ GHz. The number of channels in the equivalent multicoset sampling scheme is $p = 58$.

a frequency region $[0, F_i/2]$. However, for real signals, there is uncertainty as to whether a signal in baseband is obtained from a signal in the positive band or in the negative band.

The system parameters (number of sampling channels, sampling rates, $F_{\max}$) that were used in our last simulation are the same as those used in our optical sampling experimental setup. The fact that the simulation results were obtained in a practical situation demonstrates that our SMRS scheme can reconstruct sparse signals by using both a fewer number of sampling channels and a lower total sampling rate than are required by multicoset sampling schemes.

The number of ill-posed cases and the mean recovery runtimes for the real-valued signals are shown in Figs. 6 and 7, respectively. It can be seen that the mean rate of ill-conditioned cases is much lower for real-valued signal simulations than for complex ones. This could be due to the correlation between positive and negative frequency components of real signals. The decrease in the number of ill-conditioned cases is advantageous, since whenever there is no need to apply the pursuit algorithm the solution is obtained with confidence.

The empirical success rate of SBR4 algorithm applied to the equivalent multicoset scheme for real-valued signals is also shown in Fig. 5. It is lower than the empirical success

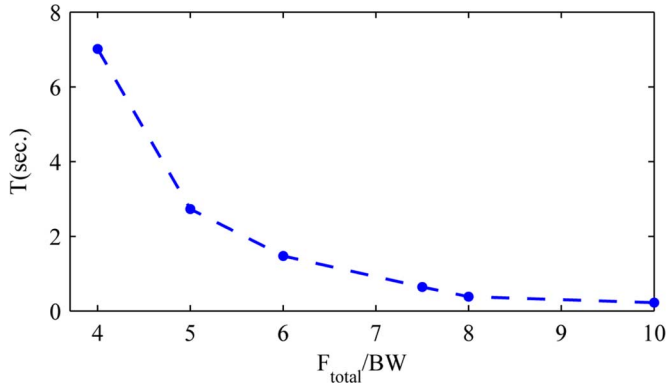

Fig. 7. Mean recovery times for equal four-band real signals for different spectral supports (total bandwidth) with $F_{\text{Nyquist}} = 40$ GHz and a total sampling rate $F_{\text{total}} = 12$ GHz.

rate of our reconstruction algorithm except for the case when the width of the bands of real-valued signals becomes very large. The SMRS requires using high-frequency resolution to obtain possible signals locations. This requirement increases the runtime. Specifically, for our simulation setup, the runtime of the SBR4 routine of [7] is smaller by a factor of about 50 than in our algorithm due to the low-frequency resolution and the smaller matrices that are used.

These results show that using the constant frequency resolution to define sparsity is less effective for the SMRS scheme than for the universal multicoset sampling scheme. The reduction procedure available in our scheme enables to define blocks adaptively according the sampled data.

B. Noisy Signals

Our algorithm's performance was also tested for its ability to reconstruct real-valued signals contaminated by Gaussian white noise. In this paper, we did not optimize the algorithm to reconstruct noisy signals. However, the presence of noise required some small modifications of the algorithm in order to reconstruct signals with a high success rate. There are several reasons for that. In a noisy environment, the noise is present in the whole signal spectrum. Therefore, the original signal can no longer be considered multiband in the strict sense. Also due to sampling at different rates each baseband signal component will contain a different noise after the downconversion. In addition, since the sampling is performed at a rate lower than the Nyquist rate, the noise from the entire spectrum is accumulated at baseband.

Our first algorithm modification is in detecting the possible bands of the originating signal. Because the spectral support of the noise is not restricted to the spectral support of the uncontaminated signal, the indicator functions in (17) cannot be directly used. Instead, we adapt (17) to noisy cases by applying a threshold similarly to [2].

Due to destructive interference between signals, some frequency components at baseband may become lower than noise. This may create some "holes" in the detected signal bands (see Appendix III). To overcome this problem, each band of the reconstructed signal was widened on each side of each detected interval in $\mathbf{S}$. The resulting widened signal support is further used to invert the corresponding sampling matrix $\hat{\mathbf{Q}}_{\mathbf{S}}$ in (13).

The solution of the linear equations given in (28) is also modified in the noisy case. Each baseband frequency f is contaminated by noise from frequencies $f + mF_i$. Not all the noise replicas are reconstructed. Therefore, in the ideal noiseless case, the error norm vanishes, whereas with a signal containing noise, one must relent on a perfect reconstruction of the DFT sequence and settle for a minimum error. In the noisy case, the solution to (28) should solve the least square problem $\min_{\mathbf{x}_S^r} ||\hat{\mathbf{x}}_S^r - \hat{\mathbf{Q}}_S^r \mathbf{x}_S^r||$ and $\min_{\mathbf{x}_S^{im}} ||\hat{\mathbf{x}}_S^{im} - \hat{\mathbf{Q}}_S^{im} \mathbf{x}_S^{im}||$. When the matrices $\hat{\mathbf{Q}}_S^{r,im}$ are not full column rank, we use the modified OMP algorithm which is adjusted to account for the errors due to noise. As noted above, in the noiseless case, one can expect a perfect reconstruction of the DFT sequence and thus the threshold error ϵ can be set to 0 or a very small number. However, with noisy signals, some care must be taken in choosing ϵ. On the one hand, if the ϵ is chosen too large, the algorithm may stop before a solution is reached. On the other hand, if ϵ is chosen too small, the reconstructed signal may include bands that are not in the originating signal thus causing the corresponding matrix to be rank-deficient. The problem of a too low threshold is solved by adding another stop criterion. Instead of stopping the algorithm only when a threshold is attained, we also check at each iteration whether the band that reduces the residual error the most causes the resulting matrix to be rank-deficient. When this occurs, the search stops and the band is not added to the matrix.

The recovery scheme was tested against real-valued signals with eight bands (four positive frequencies bands and four negative frequencies bands) contaminated by noise. The signals without noise were generated and sampled exactly as in the noiseless simulations of real signals. Noise was added at each frequency of the whole spectrum support range $[-20, 20]$ GHz. The noise had a normal distribution with standard deviation $\sigma = 0.04$; the SNR was defined by $10\log_{10}(1/(\sigma\sqrt{F_{\max}/F_2})) = 10.5$ dB, where $F_2 = 4$ GHz. This definition takes into account the accumulation of noise in baseband due to sampling. The sampling rates were the same as those in the noiseless real-valued simulations (Table I). The indicator functions $\chi_i[l]$ were constructed by applying a threshold according to [2].

Each time the modified-OMP was used the value of the threshold ϵ was chosen to be equal to $\min_{\mathbf{x}_S^r} ||\hat{\mathbf{x}}_S^r - \hat{\mathbf{Q}}_S^r \mathbf{x}_S^r||$. This value was evaluated before beginning the modified-OMP iterations.

The success was measured by the algorithm's ability to achieve a low error l_1-norm below $2\sigma\sqrt{F_{\max}/F_2} = 4.47\sigma$ for each recovered band. The mean error for each recovered band $X_{\rm rec}(f)$ and the true band $X(f)$ were evaluated as follows:

$$\frac{1}{|B|}\int_B |X_{\rm rec}(f) - X(f)|df < 2\sigma\sqrt{F_{\max}/F_2}$$

where B is the band support.

Statistics on recovering eight bands 200-MHz width each are based on 10 000 tests. The simulation show that, although the algorithm's performance inevitably decreased, it still achieved a high empirical recovery rate (37 failures out of 10 000 tests). Additional simulations were performed by changing the total bandwidth rates as was done in the simulations performed for the noiseless case. In Fig. 8, the empirical success percentage is presented for 1000 simulations of noisy signals. The results of the simulations are similar to those in the noiseless case. When the total sampling rate is eight times higher than the bandwidth rate, high success percentage was achieved. The recovery error level depended on the threshold choice. Lower threshold allows more accurate reconstruction but increases the recovery time. Different error criteria are also possible. For example, choosing l_2-norm instead of l_1-norm and setting the error threshold to be 3.3σ as in [2] resulted in 99.5% empirical success rate in recovering signals with a total bandwidth of 1.6 GHz and 99.8 percent empirical success rate for signals with a total bandwidth of 1.5 GHz.

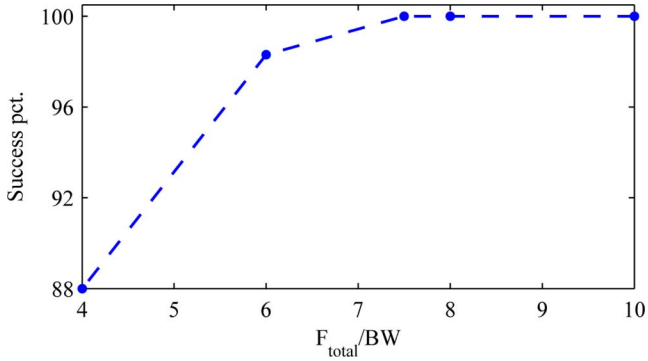

Fig. 8. Empirical success percentages for four bands of real signals noise that were contaminated with a noise with a standard deviation of $\sigma = 0.04$ for different spectral supports of the signal (BW) with $F_{\rm Nyquist} = 40$ GHz and a total sampling rate $F_{\rm total} = 12$ GHz.

Additional simulations were performed with signals suggested in [12]. The use of the Hermite polynomial shapes suggested in that work did not significantly change the reconstruction success rates in Fig. 8.

V. Conclusion

In this paper, we describe a multirate synchronous sampling scheme for blind reconstruction of sparse multiband signals using a small number of sampling channels whose total sampling rate is significantly lower than the Nyquist rate. This scheme is an alternative approach to a multicoset sampling scheme applicable when the number of sampling channel is limited. It also yields a significant improvement compared to the previously published multirate asynchronous scheme. The scheme is especially effective when the sampling rate of each sampling channel is high.

Our new reconstruction method includes a reduction procedure and a band-sparsity modification of a common pursuit algorithm. If the sampled signals possess some reasonable properties, we obtain a very high empirical reconstruction success rate.

Our sampling and reconstruction scheme has significant advantages as compared to a multicoset sampling scheme. Our algorithm provides higher empirical reconstruction success rate than the multicoset based [7] algorithm SBR4 for four-band complex signals and for four-band real signals with a total bandwidth that is less than one fifth of the total sampling rate.

Our simulations also show that the number of sampling channels in the SMRS scheme that is required to achieve high reconstruction success rate is significantly lower than required by the

multicoset sampling scheme. Only three sampling channels are required to obtain a very high reconstruction success rate with the same system parameters that are currently used in our experimental setup for electro–optical asynchronous undersampling [10].

Sufficient conditions for perfect reconstruction in SMRS scheme are provided. The sufficient conditions do not take into account that the signal is block-sparse. Therefore, very high empirical reconstruction success rates are obtained even when the sufficient conditions are not fulfilled.

We intend in the near future to implement the multirate sampling scheme in our lab for sampling signals in the frequency region of [−20, 20] GHz.

Appendix I
Real-Valued Signals

In this Appendix, we present the modifications to (11) for the real signals recovery. For simplicity, we develop the equations for $\beta = 0$. Since the signal is real valued, its Fourier transform fulfills

$$X(f) = \bar{X}(-f) \tag{21}$$

where $\overline{a+bj} = a - bj$ is the complex conjugate and a and b are real numbers.

It follows from (21) and (1) that for each channel index i all the information about $X_i(f)$ is contained in the interval $[0, F_i/2]$. Consequently, it is convenient to choose the sampling frequencies F_i such that $F_i/2 = \Delta f M_i/2$ where $M_i/2$ is an integer. Because the conjugation operation $\overline{a+jb} : a + jb \mapsto a - jb$ is not complex linear, (10) needs to be replaced with two systems of equations: one for the real part and one for the imaginary part.

We use the following notations to represent the Fourier transform of the real signals in the discretized frequencies:

$$\begin{aligned} X_i[k] &= X_i(k\Delta f), \qquad k = -\lfloor M_i/2 \rfloor, \ldots, \lfloor M_i/2 \rfloor \\ X[k] &= X(k\Delta f), \qquad k = -\lfloor M/2 \rfloor, \ldots, \lfloor M/2 \rfloor. \end{aligned} \tag{22}$$

The sequence $X_i[k]$ contains the samples of $X_i(f)$ in the baseband $[-F_i/2, F_i/2]$. The sequence $X[k]$ contains the samples of $X(f)$ given in $[-M\Delta f/2, M\Delta f/2]$, where M is chosen to fulfill $M = \lceil F_{\text{nyq}}/\Delta f \rceil$. Equation (2) now takes the following form:

$$X_i[k] = F_i \sum_{l=-\lfloor M/2 \rfloor}^{\lfloor M/2 \rfloor} X[l] \sum_{n=-\infty}^{\infty} \delta[l - (k + nM_i)]. \tag{23}$$

Equation (23) can be written in a matrix form as

$$\mathbf{x}_i = \mathbf{Q}_i \mathbf{x} \tag{24}$$

where $\mathbf{x}_i$ and $\mathbf{x}$ are given by

$$\begin{aligned} (\mathbf{x}_i)_{k+\lfloor M_i/2 \rfloor + 1} &= X_i[k]/F_i, \qquad -\lfloor M_i/2 \rfloor \le k \le \lfloor M_i/2 \rfloor \\ (\mathbf{x})_{k+\lfloor M/2 \rfloor + 1} &= X[k], \qquad -\lfloor M/2 \rfloor \le k \le \lfloor M/2 \rfloor \end{aligned} \tag{25}$$

and $\mathbf{Q}_i$ is a matrix whose elements are given by

$$(\mathbf{Q}_i)_{k+\lfloor M_i/2 \rfloor + 1, l+\lfloor M/2 \rfloor + 1} = \sum_{n=-\infty}^{\infty} \delta[l - (k + nM_i)]. \tag{26}$$

Note that, since the signal is real valued, all of its spectral information is contained in the positive frequencies.

Each element in $\mathbf{Q}_i$ is equal to either F_i or 0. Equation (24) for the different sampling channels can be concatenated as in complex signals case to yield

$$\hat{\mathbf{x}} = \hat{\mathbf{Q}} \mathbf{x}. \tag{27}$$

The Fourier transform can be decomposed into its real and imaginary parts. As a result, (27) becomes

$$\begin{aligned} \hat{\mathbf{x}}^r &= \hat{\mathbf{Q}}^r \mathbf{x}^r \\ \hat{\mathbf{x}}^{im} &= \hat{\mathbf{Q}}^{im} \mathbf{x}^{im} \end{aligned} \tag{28}$$

where $\hat{\mathbf{x}}^r = \text{Re}(\hat{\mathbf{x}})$ and $\hat{\mathbf{x}}^{im} = \text{Im}(\hat{\mathbf{x}})$. In addition, only components that correspond to positive frequencies are retained in the vectors $\hat{\mathbf{x}}^r$ and $\hat{\mathbf{x}}^{im}$. The elements of the matrices $\hat{\mathbf{Q}}^r$ and $\hat{\mathbf{Q}}^{im}$ are given by

$$\begin{aligned} \hat{\mathbf{Q}}^r_{k,\lfloor M/2 \rfloor - l + 1} &= \hat{\mathbf{Q}}_{k,l+1} + \hat{\mathbf{Q}}_{k,M-l}, \qquad l = 0, \ldots, \lfloor M/2 \rfloor \\ \hat{\mathbf{Q}}^{im}_{k,\lfloor M/2 \rfloor - l + 1} &= \hat{\mathbf{Q}}_{k,M-l} - \hat{\mathbf{Q}}_{k,l+1}, \qquad l = 0, \ldots, \lfloor M/2 \rfloor. \end{aligned} \tag{29}$$

The reconstruction is performed with (28) exactly as in the complex case.

Appendix II
Reduction Procedure

In this Appendix, we explain the idea behind the reduction procedure. By using the multirate sampling scheme, it is possible to obtain a set of possible signals locations and thus to reduce the sampling matrix $\hat{\mathbf{Q}}$.

Consider a complex signal consisting of a single signal frequency f_0. Due to the sampling theorem sampling with rate F_i, the original frequency f_0 aliases to the baseband frequency f_i

$$f_i = f_0 - m_i^* F_i \tag{30}$$

where m_i^* is an integer such that $f_i \in [0, F_i]$.

The observed frequency f_i originates from a set of possible locations at

$$f_0^{i,j} = f_i + m_i^j F_i, \qquad m_i^j \in \mathbf{Z}. \tag{31}$$

For $m_i^j = m_i^*$, we obtain the original frequency f_0.

By sampling the signal at P different rates $\{F_i\}_{i=1}^P$, the set of all possible signals locations is obtained by taking the intersection of possible locations resulting at sampling channel i (31)

$$S_0 = \bigcap_i \bigcup_j f_0^{i,j}. \tag{32}$$

Thus, any $f \in S_0$ fulfills (31) for every $1 \leq i \leq P$ and also $f_0 \in S_0$.

By applying a multiband signal model Property 1 on signal bands edges, one obtains a set of possible signal bands locations. Consider a multiband signal that occupies a union of intervals $\bigcup_{n=1}^{N}(a_n, b_n]$ on the frequency axis. For channel i with sampling rate F_i, the possible signals locations are given by the set

$$S_i = \bigcup_m \bigcup_{n=1}^{N} (a_n + mF_i, b_n + mF_i]. \tag{33}$$

By sampling with P sampling rates, a smaller set of possible locations S is obtained by taking the intersection of S_i

$$S = \bigcap_{i=1}^{P} S_i = \bigcap_{i=1}^{P} \bigcup_m \bigcup_{n=1}^{N} (a_n + mF_i, b_n + mF_i]. \tag{34}$$

It follows from (34) that S has a multiband structure. It also contains the original signal bands as shown for a single frequency. This structure is used in the modified-OMP algorithm to identify the minimum subset of S that contains the original signal support.

In some cases, the resulting disjoint intervals of S are larger than the signal bands themselves. This is resolved only after the original signal shape is recovered. Only then the true support is obtained.

Appendix III
Reduction Procedure Analysis in Noisy Environment

In this Appendix, we analyze the performance of the reduction procedure in the noisy environment. There are cases in which some frequency components of the original signal can sum up to an amplitude which is lower than noise. This could cause such signals to be undetected. Signals can also be undetected if it they are canceled out by noise.

Consider the observed signal at some baseband frequency $k_0\Delta f$ of the ith channel $X_i[k_0]$. The sequence $\{X[l]\}_{k_0+kM_i}$ of the DFT values of some noiseless signal is downconverted to the same baseband frequency $k_0\Delta f$. The maximum length of the sequence is $N = \lceil F_{\max}/F_i \rceil$. Also assume that the signal is contaminated by some noise sequence $\{n_m\}$. The DFT value at the baseband frequency $k_0\Delta f$ at ith channel is

$$y = X_i[k_0] = \sum_m (X[k_0 + mM_i] + n_m). \tag{35}$$

For some threshold ϵ, the probability of misdetecting a signal in a given baseband frequency is

$$P_\epsilon = P(|y| \leq \epsilon). \tag{36}$$

We have performed simulations with the same signal profiles that were used in our real signal simulations (20) for different bandwidths (50, 100, 150, and 200 MHz). The signals were generated as in our noisy signals simulations section with SNR = 10.5 dB. Each signal consisted of four equal size bands (eight for positive and negative frequencies). We calculated the empirical rate of misdetecting a signal frequency in our reduction procedure.

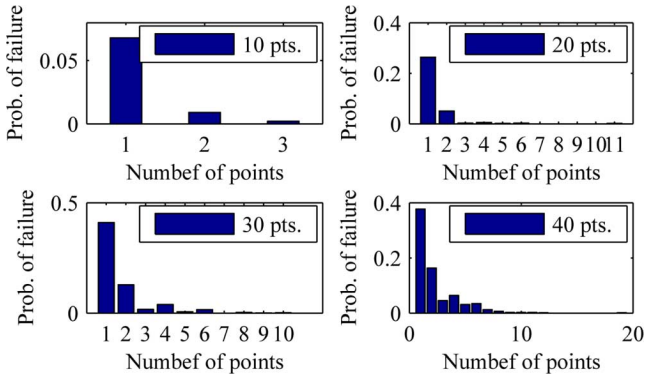

Fig. 9. Probability of misdetecting points in one band. Real-valued four-band (eight positive and negative frequencies) signals sampled with rates of 3.8, 4.0, and 4.2 GHz with SNR of 10.5 dB at baseband. Each band shape is given by (20). The number of discrete points in each signal band is given in the legend.

Fig. 9 shows the probability of misdetecting a given number of points in a single band. The number of discrete points of each signal band is shown in the legend (one bandwidth/Δf). The x-axis indicates the number of misdetected points, and the y-axis shows the corresponding probability of misdetection.

To resolve this misdetection, the bands were widened on each size by 10% such that the total bandwidth increased by 20%. Blocks which contained less than ten points were widened on each side to contain exactly ten points. By using such simple method, we were able to recover the vast majority of points that were misdetected in a reduction procedure (94% for signals with 200-MHz bands and 100% for the rest of the signals).

Additional simulations were performed with signals suggested in [12]. The use of the Hermite polynomial shapes suggested in that work did not significantly change the results presented in Fig. 9.

References

[1] A. Zeitouny, A. Feldser, and M. Horowitz, "Optical sampling of narrowband microwave signals using pulses generated by electroabsorption modulators," *Opt. Commun.*, vol. 256, pp. 248–255, Dec. 2005.

[2] A. Rosenthal, A. Linden, and M. Horowitz, "Multirate asynchronous sampling of sparse multiband signals," *J. Opt. Soc. Amer. A*, vol. 25, pp. 2320–2330, Aug. 2008.

[3] A. Kohlenberg, "Exact interpolation of band-limited functions," *Appl. Phys.*, vol. 24, pp. 1432–1436, 1953.

[4] P. Feng and Y. Bresler, "Spectrum-blind minimum-rate sampling and reconstruction of multiband signals," in *Proc. IEEE Int. Conf. Acoust. Speech Signal Process.*, May 1996, vol. 3, pp. 1688–1691.

[5] R. Venkantaramani and Y. Bresler, "Optimal sub-Nyquist nonuniform sampling and reconstruction for multiband signals," *IEEE Trans. Signal Process.*, vol. 49, no. 10, pp. 2301–2313, Oct. 2001.

[6] Y. M. Lu and M. N. Do, "A theory for sampling signals from a union of sub-spaces," *IEEE Trans. Signal Process.*, vol. 56, no. 6, pp. 2334–2345, Jun. 2008.

[7] M. Mishali and Y. Eldar, "Blind multiband signal recostruction: Compressed sensing for analog signals," *IEEE Trans. Signal Process.*, vol. 57, no. 3, pp. 993–1009, Mar. 2009.

[8] E. Candes and M. Wakin, "An introduction to compressive sampling," *IEEE Signal Process. Mag.*, vol. 25, no. 2, pp. 21–30, Mar. 2008.

[9] A. M. Bruckstein, D. L. Donoho, and M. Elad, "From sparse solutions of systems of equations to sparse modeling of signals and images," *SIAM Rev.*, vol. 51, no. 1, pp. 34–81, 2009.

[10] A. Feldster, Y. P. Shapira, M. Horowitz, A. Rosenthal, S. Zach, and L. Singer, "Optical under-sampling and reconstruction of several bandwidth-limited signals," *J. Lightw. Technol.*, vol. 27, no. 8, pp. 1027–1033, Apr. 2009.
[11] R. Penrose, "A generalized inverse for matrices," *Proc. Cambridge Philosoph. Soc.*, vol. 51, pp. 406–413, 1955.
[12] G. de Abreu, C. JohnMitchell, and R. Kohno, "Jitter-robust orthogonal Hermite pulses for ultra-wideband impulse radio communications," *EURASIP J. Appl. Signal Process.*, vol. 2005, pp. 369–381, Jan. 2005.

Michael Fleyer received the B.Sc. degree in electrical engineering from the Technion—Israel Institute of Technology, Haifa, Israel, in 2004, where he is currently working towards the M.Sc. degree at the Department of Electrical Engineering.

Alexander Linden received the Ph.D. degree in mathematics from the University of Michigan, Ann Arbor, in 1998.

He was a recipient of a Rackham Graduate Fellowship and a John and Fanny Hertz Fellowship. He has held positions in the Mathematics Departments at Brown University, Indiana University, University of Canberra, and is currently a Research Associate at the Department of Electrical Engineering, Technion—Israel Institute of Technology, Haifa, Israel. He has published papers in graph theory, differential equations, satellite system design, and signal processing. He has worked at ANSER providing technical consulting to the United States Department of Defense.

Moshe Horowitz received the Ph.D. degree in electrical engineering from the Technion—Israel Institute of Technology, Haifa, Israel, in 1994.

Since 1997, he has been a faculty member at the Department of Electrical Engineering, Technion. His current research interest includes inverse scattering theory in fiber gratings, nonlinear optical effects, novel fiber lasers, and microwave photonics.

Amir Rosenthal was born in Haifa, Israel, in 1981. He received the B.Sc. and Ph.D. degrees in electrical engineering from the Department of Electrical Engineering, Technion—Israel Institute of Technology, Haifa, Israel, in 2002 and 2006, respectively.

Currently, he is a Postdoctoral Fellow at the Institute for Biological and Medical Imaging (IBMI), Technische Universitaet and Helmholtz Zentrum Muenchen, Munich, Germany. His research interests include optoacoustic imaging, inverse problems, and optical modeling.